Study of radiative and kinetic properties of femtosecond laser ablated brass plasma by optical emission spectroscopy

P. Mathi [*], Vinu. V. Namboodiri and Ajay K. Singh

Radiation & Photochemistry Division,
Bhabha Atomic Research Centre, Mumbai-85, India

[*]*Corresponding author E-mail:* mathip@barc.gov.in

(Received 14 June 2015, Published 09 July 2015)

Abstract

Femtosecond laser induced plasma (LIP) in brass was characterized by optical emission spectroscopy (OES). The LIP spectra is dominated by emission from excited neutral species of Cu and Zn. The ionic emission lines are found to decay more rapidly compared to the atomic emission lines. Time resolved OES studies on the expanding plasma plume have provided some insight into probable excitation pathways and the temporal behavior of the excited species.

Further assuming local thermodynamic equilibrium (LTE), the fs-LIP source was characterized for excitation temperature and electron number densities by using the Boltzmann plot method and the width of Stark broadened line profiles respectively. The influence of laser fluence on excitation temperature and electron density was also investigated. The emission intensities exhibit two ablation regimes corresponding to ablation dominated by optical penetration depth at low fluence and by electron thermal diffusion length at higher fluence. Comparative studies on the behavior of copper emission lines from both pure copper and brass samples suggest that femtosecond laser pulses might mitigate the matrix effect in the ablation process.

Keywords: Optical emission spectroscopy, Laser induced breakdown spectroscopy, Laser induced plasma, Femtosecond laser ablation, Time resolved emission

1. Introduction

Laser induced breakdown spectroscopy (LIBS), a spectroscopic technique used to identify constituents of an unknown sample, involves ablating a small quantity of the sample and monitoring the subsequent emission from atomic and molecular species. Its applicability for qualitative and quantitative estimation of the compositions of solids, liquids, and gaseous samples has made it a popular analytical tool. In particular, LIBS has been widely employed for elemental composition analysis of metallurgical samples. The direct solid sampling method [1,2] precludes any rigorous sample pretreatment procedures thus minimizing the risk of sample contamination as compared to other analytical methods that involve digesting solids into solution [3-5] and consumes small amounts of material (few picograms). The simultaneous multi-element detection capability

of this technique and its sensitivity to a wide variety of elements makes it a versatile and attractive analytical method.

Conventional LIBS systems have employed solid state Nd:YAG lasers with nanosecond (ns) pulse duration and pulse energies ≥ 10 mJ. The laser - matter interaction (for metallic samples) begins with rapid heating of the free electron gas of a metal due to inverse Bremsstrahlung and avalanche (collisions) ionization, followed by energy transfer from the hot electron gas to the lattice and heat transfer from the electrons to the bulk. These processes lead to the formation of a temperature field and depending on the temperature attained, the material melts, evaporates or is transferred to a plasma state. Ablation results from both evaporation and melt expulsion. The typical characteristic time scales of the different processes involved in laser-matter interaction are: free electron heating and thermalization takes approximately 100fs; cooling of the hot electron gas and energy transfer to the lattice takes a few picoseconds; thermal diffusion in the bulk takes place on a time scale of 10^{-11}s; and onset of thermal melting and ablation occurs [6-8] after 10^{-10}s. In case of ablation with ns-pulses, the initial part of the pulse encounters a target having well defined optical and mechanical properties, but as energy deposition proceeds, melting and evaporation take place. The ns-laser pulse interacts with different transient thermodynamic states which hinders the analytical performance of this technique. Firstly, it is an important source of non-reproducibility in the ns-ablation process. Secondly, it poses serious challenges in a sample containing elements with different melting temperatures. As the major part of the evaporated material comes from molten metal, there is a high probability for preferential volatilization (fractionation) to occur [9] consequently the composition of the ablated mass will not reflect the stoichiometry of the sample. Thirdly, the ns-plasma is very highly ionized since a significant proportion of the later part of the energy pulse goes into heating the plasma formed during the earlier part of the pulse through linear absorption, this results in large amounts of continuum emission, especially at short time scales, making it difficult to observe short lived species [10]. Another shortcoming in ablating with ns pulses is the large heat affected zone (HAZ) which extends beyond the irradiated volume because of thermal diffusion during the irradiation time scale [11,12], this limits the spatial and depth resolution. These critical challenges can be addressed by using intense fs laser pulses [13,14]. In case of fs-laser ablation, the laser pulse interacts only with the electron sub-system of a material. Since the pulse width is shorter than the electron relaxation time in the lattice, all laser energy is deposited onto the target. In other words, the laser pulse is over before the material undergoes any changes in thermodynamic state. Material removal / ablation begins on the order of picoseconds after the laser pulse. This results in improved ablation reproducibility [15]. Further, several reports [16-18] suggest that the use of ultrashort pulses might mitigate the matrix effect in the ablation process. Additionally, the heat affected zone (HAZ) around a fs-pulse induced crater was reported to be undetectable by TEM [11]. This is due to the limited thermal diffusion into the surrounding volume during the time scale of irradiation. Thus ablation with fs-lasers can hugely enhance the analytical capability of LIBS.

The high-power fs-laser systems required for this purpose are relatively huge and complicated systems and only recently such systems have become available commercially. The work reported here involves a systematic investigation of the kinematic and radiative properties of fs-laser ablated brass plasma by applying optical emission spectroscopy (OES). The experiments were performed with brass sample. Brass is a binary alloy characterized by a significant difference in thermal properties of the main components, copper and zinc; hence it is a good example to investigate ablation characteristics.

2. Experimental section

The 1kHz femtosecond laser system employed in the present work comprises of a Kerr lens mode locked Ti-sapphire oscillator, a 1KHz chirped pulse regenerative amplifier and a grating Compressor (Amplitude Technologies, France). The Ti-Sapphire oscillator is optically pumped by a CW frequency doubled

Nd:YVO4 laser (5W @ 532nm, optically pumped semiconductor pump laser).The oscillator spectrum is centered at 792nm with a FWHM of approximately 60nm. The power level of the short pulse oscillator is ~ 420mW @ 80MHz repetition rate. The seed beam is routed into the stretcher and is subsequently amplified in the Chirped Pulse Amplifier (CPA). The later module includes the regenerative amplifier and the multipass amplifier. A Nd:YLF laser (1kHz @ 527nm) produces the gain in both the regenerative amplifier and the multipass amplifier. The amplified output is ~ 4.5W. Following amplification, the pulses are re-compressed in the compressor. The final output from the compressor is a train of 1kHz pulses (3.3mJ/pulse, 50fs FWHM) centered at 800nm. The pulse-to-pulse energy stability of the femtosecond laser output was about 5%. An important feature in fs-laser ablation experiments is the ratio of post- and pre-pulse intensities relative to the intensity of the main pulse (these are connected to the process of amplification); in our system this was found to be better than $1.6*10^2$:1 and $1.7*10^3$:1, respectively. The pulse duration of the fs-pulses was measured with an autocorrelator (PulseCheck, APE GmbH, Germany).

Plasma for LIBS analysis is generated by focusing 1mJ of energy onto the sample surface using a BK7 planoconvex lens (f=10cm). The samples were mounted on a motorized Y-Z translational stage which is interfaced to LabVIEW and provides automated sample translation during data acquisition. Collection of plasma emission was done with a collimator which was fibre-coupled to an Echelle grating spectrograph (Andor Mechelle ME5000). The cross dispersion Echelle spectrograph covers the spectral range from 200–830nm in one scan with 0.1nm resolution. This, in conjunction with a thermoelectric cooled ICCD (Andor DH734-18mm-CCI-01U) which is sensitive in the UV-VIS-NIR is used for the acquisition of spectra. The ICCD was gated in synchronization with the fs-laser pulse. The gate delay, gate width and the detection system were computer controlled through a digital delay generator. The wavelength calibration of the spectrograph – ICCD was done using the NIST certified low pressure Hg-Ar lamp which gives narrow emission lines from 200–1000nm with accurately known wavelengths. The intensity calibration was done using the NIST certified Deuterium-Quartz-Tungsten-Halogen lamp.

3. Results and Discussion

The plasma plume generated by fs-laser ablation of a brass sample is characterized by optical emission spectroscopy. Emission features specific to atomic and ionic species of Cu and Zn and the corresponding line emission kinetics are described in Section 3.1. In Section 3.2, with the aid of time-resolved spectra of neutral atom line emissions, two important plasma parameters namely temperature and electron number density are estimated from spectral intensities and line widths. Finally, in Section 3.3, the effect of laser fluence on the plasma parameters is presented, further the behavior of copper emission lines from both pure copper and brass samples have been compared to see if there is any difference due to matrix effects.

3.1 Spectral Emission Features

Fig.1a shows the fs-laser induced plasma emission spectra of brass recorded in air after a delay of 100ns wrt the excitation pulse, using an integration time of 1200ns. Various transitions corresponding to the emissions from ionic and atomic species were identified using the NIST database [19].

Ionic emission lines

The emission lines at 224.2nm and 224.7nm (Fig.1b, inset of Fig.1a) are assigned to the $3d^9 4p$-$3d^9 4s$ electronic transition of copper ion. The excitation energies for this transition ranges from 8.2 to 9.4eV. The emission lines at 255.8nm and 250.2nm (Fig.1b, inset of Fig.1a) correspond to Zn(II) transitions from $3d^{10}5s$ - $3d^{10}4p$ energy levels and the excitation energies for this transition ranges from 4.84 to 4.88eV.

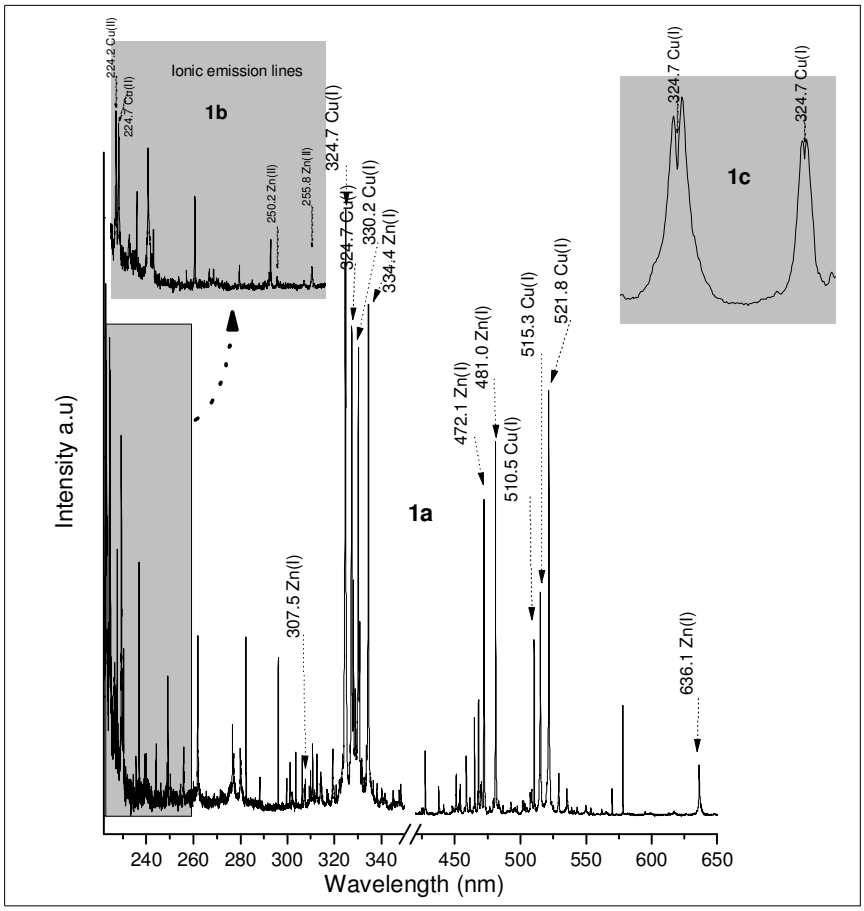

Fig.1a fs-laser induced plasma emission spectrum of brass recorded in air; gate delay: 100ns, gate width 1200ns

Fig.1b (inset) Ionic emission lines of Cu and Zn species

Fig.1c (inset) self reversal observed in Cu(I) 324.7nm and 327.4nm

Atomic emission lines

The LIP emission spectra of brass is dominated by the strong lines of Cu(I) transitions at 324.3□, 324.7, 510.5, 515.3, 521.8nm and Zn(I) transitions at 330.2, 334.4, 472.1, 481.0 nm and 636.1nm. The strong emission features at 324.7nm and 327.4nm involve the transition of the Cu atom from the higher energy level $3d^{10}4p^1$ to the lower energy level $3d^{10}4s^1$ (P-S type) and occur early into the life of the plasma. These Cu(I) emissions ending in the ground state are particularly susceptible to self-absorption and in more extreme cases can be self-reversed. The otherwise single lines at 324.7nm and 327.4nm appear to have a dip at the central frequency (Fig.1c, inset of Fig.1a). As the excited atoms in the central core of the plasma decay to the ground state, the emitted photons corresponding to resonance transitions have a high probability of being absorbed by the 'cooler' atoms in the outer layer of the plasma, thereby reducing the observed intensity of the emission line. These lines exhibit broadening due to high free electron density, have large widths and hence are not taken into account for estimation of plasma parameters. The other persistent Cu(I) transition at 510.5nm (from $3d^{10}4p^1$ to $3d^94s^2$) that starts at the earliest moment in the life of plasma involves the terms P-D. The transitions involving terms D-P (transitions from $3d^{10}4d^1$ to $3d^{10}4p^1$) occur later in time as compared to those appearing at wavelengths 515.3nm

and 521.8nm. The simultaneously persistent and resonant zinc line (transition from $4s^2$ to $4s^14p^1$), with emission at 307.5nm was observed with a meagre intensity. Zn(I) lines of the D-P type at 334.5nm, 636.2nm for zinc (from $4s^14d^1$ to $4s^14p^1$) and at 280.1nm (from $4s^15d^1$ to $4s^14p^1$) are clearly observed, the later has a very large line width. Other persistent Zn(I) lines include the triple line emissions at 468.0nm, 472.2nm, and 481.0nm which belong to the S-P transitions ($4s^15s^1$ to $4s^14p^1$); these lines are relatively narrower. It may be also noted that the typical molecular nitrogen emission at 337.1nm, O(I) at 394nm, N(I) at 414nm, O(II) at 407.6nm and N(II) at 399.5nm arising from ambient air breakdown [20] are absent under the present conditions. This absence of air breakdown will be helpful in identifying certain emission lines in this region which otherwise could have been assigned to ambient oxygen and nitrogen.

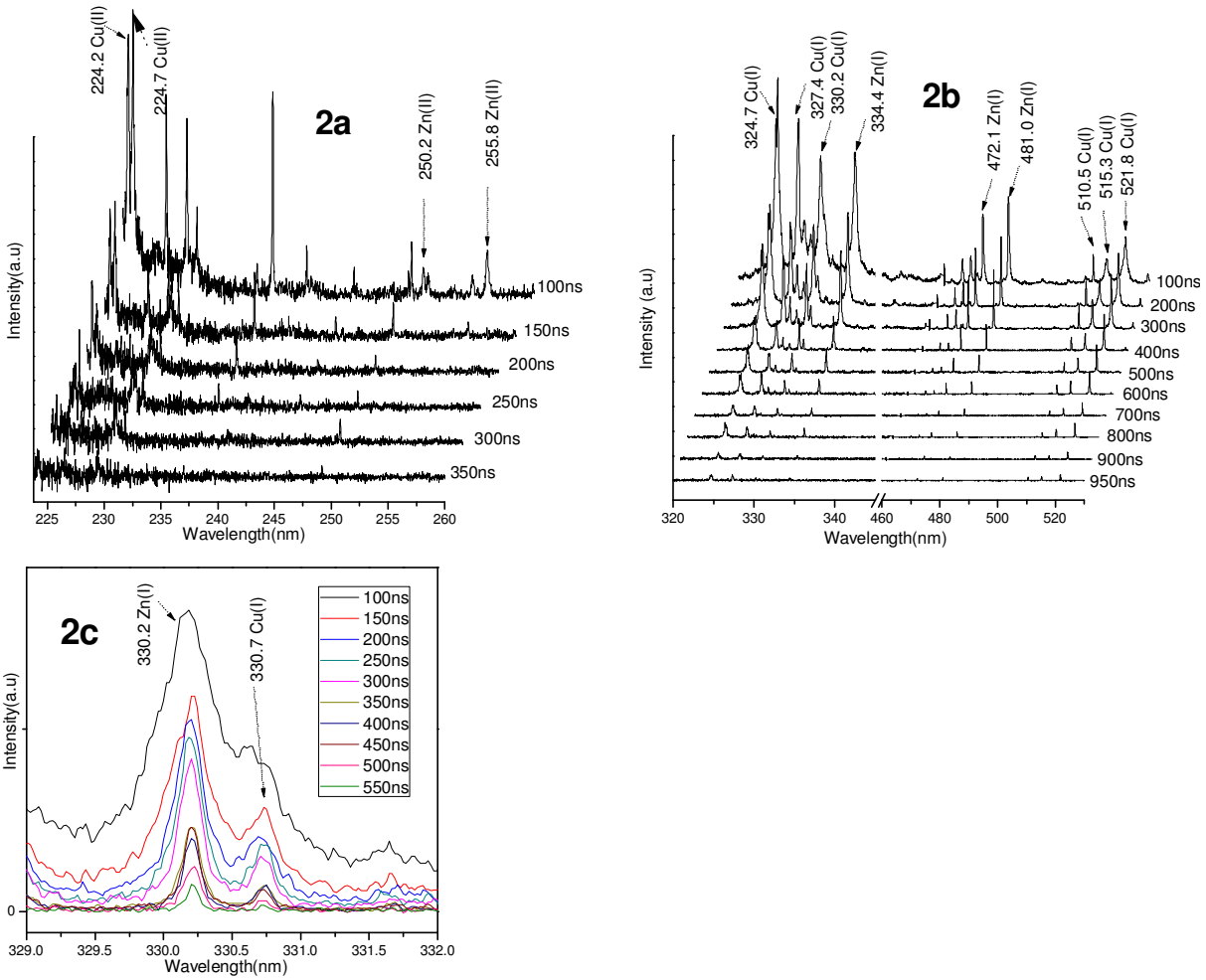

Fig.2a, 2b Variations in the time resolved emission spectrum of plasma plume.
(**2a**: spectral region: 224-260nm, **2b**: spectral region: 320-530nm)
Ionic emission lines are found to decay more rapidly compared to atomic emission lines

Fig.2c Overlapping emission lines of Zn(I) 330.2nm and Cu(I) 330.7nm become resolved as the plasma cools down

In order to get more insight into the temporal behavior of the excited species and identifying the possible excitation mechanisms, we have carried out time resolved OES studies on the expanding plasma plume. A short integration time (gate width=50ns) was used for the time-resolved measurements of the different plasma

parameters while the time delay was varied in steps of 50ns from an initial delay of 100ns. Fig.2a and 2b show variations in the time resolved emission spectra of the plume. Investigations on the plasma plume from the time of its initiation could not be carried out due to the strong continuum background. The spectra recorded at short delay times is dominated by strong continuum background which arises from bremsstrahlung process, collisions of electrons with ions and atoms (free–free emission), and recombination of electrons and ions (free–bound emission). The continuum drops rapidly because of the expansion and cooling of the plasma. The time-resolved spectra shown in Fig.2a and 2b are characterized by rapid reduction in the emission intensities. The ionic emission lines are found to decay more rapidly compared to the atomic emission lines. The Zn(II) line at 250.2nm disappears before 150ns while the other Zn(II) emission line at 255.8nm could be observed upto 200ns into the life of plasma. The Zn(I) atomic emission lines at 481nm could be observed upto 950ns. The Cu(II) lines at 224.2nm and 224.7nm are seen upto 200ns whereas the copper atomic resonance lines at 324.7nm and 327.4nm can be observed upto 950ns. The time-resolved emission profile follows variations of the plasma and provides clue to the various excitation processes that might take place within a plasma plume. These Cu(II) and Zn(II) ionic species require higher excitation energies (plus the ionization energy of Cu / Zn atom); they are most likely produced through collisions with highly-energetic particles in the breakdown zone [21], as indicated in Eq.(1a and 1b);

$$Cu \rightarrow Cu^{+} \rightarrow Cu^{Z+} \quad (1a)$$

$$Zn \rightarrow Zn^{+} \rightarrow Zn^{Z+} \quad (1b)$$

However, as the plasma expands, the number density of these particles having sufficient kinetic energy to excite their excited levels decreases, hence the rapid decrease in emission intensities of ionic species. Further as the expansion proceeds, various recombination reactions such as Eq.(2a and 2b) become more dominant. Such reactions lead to generation of excited species.

$$Cu^{+} + e^{-} \rightarrow Cu^{*} + \Delta E_1 \quad (2a)$$

$$Zn^{+} + e^{-} \rightarrow Zn^{*} + \Delta E_2 \quad (2b)$$

where Cu* and Zn* are the excited states of neutral species. These species emit characteristic radiation along with the electron-ion recombinations which yield continuum background over a wide wavelength range. These excited species can be produced via another route such as direct collisional excitations within the plasma plume:

$$Cu + e^{-}_{fast} \text{ or } M_{fast} \rightarrow Cu^{*} + e^{-}_{slow} \text{ or } M_{slow} \quad (3a)$$

$$Zn + e^{-}_{fast} \text{ or } M_{fast} \rightarrow Zn^{*} + e^{-}_{slow} \text{ or } M_{slow} \quad (3b)$$

where e^{-}_{fast} and M_{fast} denote an electron and a particle having enough kinetic energy to excite Cu or Zn. The number density of highly-energetic particles and electrons decreases as the plasma plume expands, therefore, collisions of the type indicated in Eq.(3a and 3b), take place less frequently. On the other hand, atomic emission lines which require small excitation energies can be formed through various de-excitation processes such as a stepwise de-excitation process (Eq.4) as well as by recombination collision (Eq.5):

$$Cu^{2*}_{\text{higher excited level}} \rightarrow Cu^{1}*_{\text{lower excited level}} + h\nu \quad (4a)$$

$$Zn^{2}*_{\text{higher excited level}} \rightarrow Zn^{1}*_{\text{lower excited level}} + h\nu \quad (4b)$$

$$Cu^{+} + e^{-}_{secondary} \rightarrow Cu^{*}_{excited} \quad (5a)$$

$$Zn^{+} + e^{-}_{secondary} \rightarrow Zn^{*}_{excited} \quad (5b)$$

These species may also be created in the expansion zone of fs-LIP through recombination and de-excitation processes of highly excited species initially created in the breakdown zone, as indicated in Eqs.(4) and (5); this might explain the longer persistence of the Cu(I) and Zn(I) emission lines as compared to Cu(II) and Zn(II) lines respectively (cf. Fig.3a and 3b). Further the estimated life times for the Zn(I) 481.0nm ($4s5s^3S_1 \rightarrow 4s4p^3P_2$) and Cu(I) lines 510.5nm ($4p^2P_{3/2} \rightarrow 4s^2D_{5/2}$) were found to be 172ns and 303ns respectively. This difference in life times can be ascribed to the difference in upper excited energy level for the species: 6.66eV for Zn(I) and 3.82eV for Cu(I).

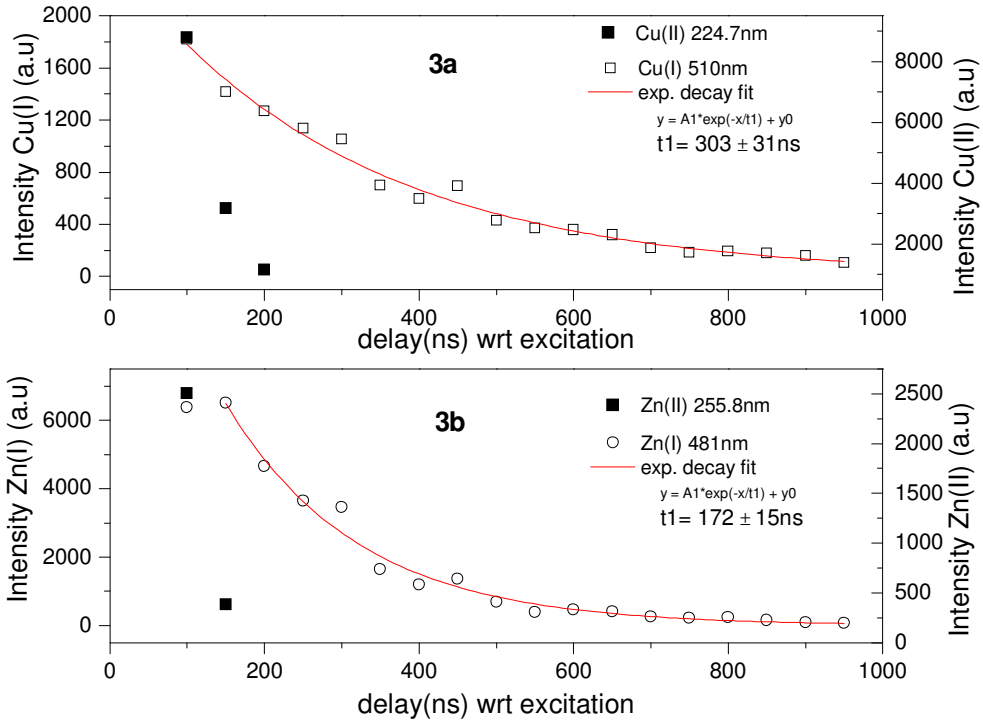

Fig. 3a, 3b Temporal evolution of persistent copper (510.5 nm) transitions ($4p^2P_{3/2} \rightarrow 4s^2\,^2D_{5/2}$) (3a) and Zn lines (481.0 nm) transitions ($4s5s^3S_1 \rightarrow 4s4p^3P_2$) (3b). The mean decay time for the Zn(I) transition is 172ns whereas it is 302ns for Cu(I) transition

Time resolved spectra also help in resolving closely spaced overlapping lines. In general, for elemental analysis, the spectral resolution of the spectrometer plays a crucial role, our Echelle grating spectrometer has a resolution of ~ 0.1nm which helps in identifying different elements with close by emission lines. However, in the case of laser induced plasma, the properties of the plasma play an equally important role along with the dispersive power of the spectrometer. For example, the neutral emission lines of Zn(I) at 330.2nm and Cu(I) at 330.7nm have a wavelength difference that can be, in principle, resolved by our spectrometer. However, as seen in the LIP emission spectra Fig.2c, during the initial moments into the life of plasma (up to 100 ns), these lines are very wide and overlapping. This is due to high electron density and the large number of collisions which lead to continuum bremsstrahlung radiation. This poses difficulty in identification / assignment of various lines. During the later stages of the plasma (spectrum recorded after a delay of ~200ns), with the decrease of the continuum radiation these lines become clearly distinguishable.

3.2. Estimation of excitation temperature and electron number density

The laser induced multi-element plasma is continuously evolving with time. In order to extract quantitative analytical information from the plasma, a thorough knowledge of the population distribution in various atomic /ionic electronic levels will be required. This approach will involve rigorous description of all the kinetic processes taking place in the plasma. A simplified thermodynamic route to quantitative interpretation of the plasma for analytical quantification purposes was proposed by van der Mullen, wherein one can describe the

system through the Saha-Eggert and Maxwell / Boltzmann distribution by using parameters such as electron / excitation temperature and electron number density [22].

3.2a Estimation of excitation temperature

Plasma excitation temperature T_{ex} is determined using the Boltzmann plot method [23,24]. The validity of this method for temperature estimation is based on the assumption that (i) local thermodynamic equilibrium (LTE) prevails in the plasma plume in which case the atomic and ionic states should be populated and depopulated predominantly by the electron collisions, rather than by radiative processes and (ii) the plasma should be optically thin for the lines that are used for its characterization (meaning that all the emitted photons should escape the plasma volume); verification of these criteria is discussed at the end of this section. Under such conditions, the relative populations of excited levels in an atom / ion i.e the Atomic State Distribution Function (ASDF) is described by the Boltzmann distribution [23,24]:

$$\frac{n_k^z}{n^Z} = \frac{g_k^Z}{U(T_{ex})} e^{-E_k^Z / k_B(T_{ex})} \qquad (1)$$

where n_k^z, g_k^Z and E_k^Z are the population, degeneracy and energy of the upper energy level k respectively; n^Z is the number density and $U(T_{ex})$ is the partition function of the species in the ionization stage Z(= 0 and 1 for neutral and singly ionized atoms respectively), k_B is the Boltzmann constant and T_{ex} is the excitation temperature characterizing the ASDF. The integrated intensity of the transition I_{ki}^Z from upper energy level k with energy E_k^Z to lower energy level i of the species is given by:

$$I_{ki}^Z = \frac{hc}{4\pi\lambda_{ki}^Z} A_{ki}^Z n_k^Z L \qquad (2)$$

where λ_{ki}^Z is the wavelength of the corresponding transition A_{ki}^Z is the transition probability and L is the characteristic length of the plasma. Eq.(1) and (2) can be combined and rewritten as:

$$\ln\left(\frac{I_{ki}^Z \lambda_{ki}^Z}{g_k^Z A_{ki}^Z}\right) = -\frac{1}{k_B T_{ex}} E_k^Z + \ln\left(\frac{hcLn^Z}{4\pi U(T_{ex})}\right) \qquad (3)$$

The excitation temperature is deduced from Boltzmann diagrams built from a large number of spatially integrated neutral Cu(I) (578.2, 510.5, 515.3, 521.8, 465.1 and 427.5nm) and Zn(I) emission lines (468.0, 472.3, 481.0, 636.3, 330.2, 334.4nm) which are well resolved and free from spectral interference; the relevant spectroscopic parameters are listed in Table 1. T_{ex} is determined from the slope of $\ln\left(\frac{I_{ki}^Z \lambda_{ki}^Z}{g_k^Z A_{ki}^Z}\right)$ Vs E_k^Z. The temporal evolution of plasma excitation temperature for both Cu(I) and Zn(I) species is shown in Fig.4a. The overall uncertainty in determination of the excitation temperature is ~ 10% due to inherent uncertainties in the transition probabilities and the integrated line intensities used in the Boltzmann plots, The estimated temperatures using Cu(I) lines (510.5nm) is higher compared to Zn(I) transitions (481.1nm), this may be due to the higher heat of vaporization for Cu compared to Zn (heat of vaporization 3630J/g of Cu and 1746.44J/g of Zn; vaporization temperature: 2595°C for Cu and 906°C for Zn). The excitation temperature data was fitted with a power function of the form: $\psi(t) = at^b$, where $\psi(t)$ represents excitation temperature as a function of time t, a is the coefficient, and b is the exponential parameter defining the rate of decay. In order to have better comparison between exponential decay values, the coefficient of the power function "a", was fixed for both Cu and Zn cases. The figures show that the plasma cools down exponentially after about 200ns.

Table 1: Spectroscopic parameters of prominent Cu(I) and Zn(I) lines

Wavelength (nm)	Upper energy Level (eV)	Lower energy level (eV)	degeneracy upper level g_k	Transition Probability A_{ki} (s^{-1})
Cu(I)				
578.19388	3.79	1.64	2	1.9E6
510.53163	3.82	1.39	4	1.95E6
515.247	6.19	3.79	4	1.03E8
521.74795	6.19	3.82	6	1.22E8
465.11927	7.74	5.07	8	4.19E7
427.5056	7.74	4.84	8	3.176E7
Zn(I)				
468.03497	6.655	4.01	3	1.553E7
472.25331	6.655	4.03	3	4.576E7
481.07371	6.655	4.08	3	7.004E7
636.34232	7.74	5.80	5	4.652E7
330.247	7.78	4.03	5	1.07E8
334.51313	7.78	4.08	7	1.5E8

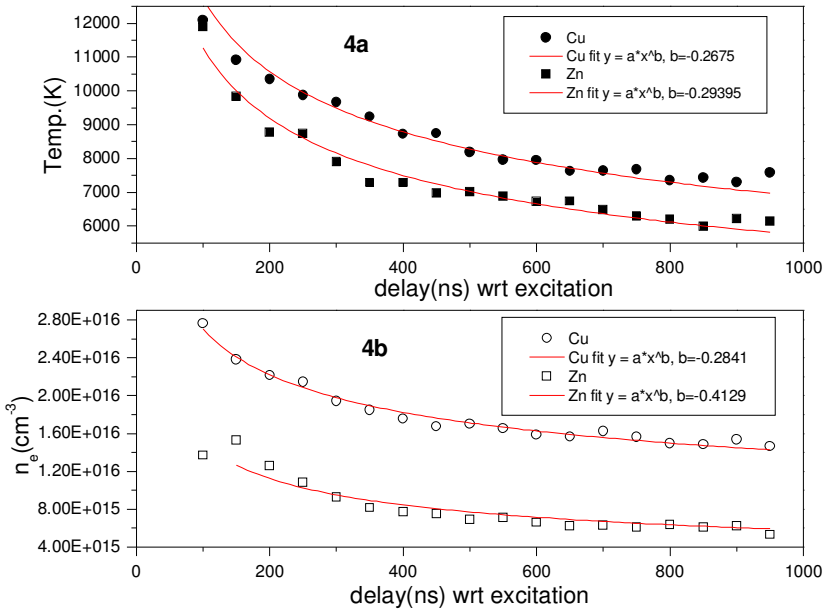

Fig.4a Temporal evolution of plasma temperature for Cu(I) and Zn(I) species

Fig.4b Temporal evolution of electron density for Cu(I) (510.5nm) and Zn(I) (481.0nm) transitions

3.2b Estimation of electron number density

Electron number density n_e is a crucial parameter for describing the plasma environment and also for establishing thermodynamic equilibrium. One of the diagnostic methods for measuring n_e is based on Stark broadening of emission lines [24]. Under the present experimental conditions of a LIP, the broadening observed in the emission line profiles can be attributed to three different mechanisms namely Doppler broadening, resonance pressure broadening and Stark broadening [25]. The Doppler width in emission lines arises from the random thermal motion of the emitter and depends on the absolute temperature and atomic mass of the emitting species. The Doppler width (FWHM) is estimated by:

$$FWHM = 7.16 * 10^{-7} \lambda \sqrt{\left(\frac{T_e}{M}\right)} \quad (4)$$

where T_e (K) is the electron temperature (in LTE, $T_{ex} = T_e$), M is the atomic mass and λ is in nm. The Doppler width corresponding to Cu(I) emission at 510.5nm and Zn(I) emission at 481nm with T_{ex} = 11000K is estimated to be 0.0048nm and 0.0045nm respectively. This is negligible compared to the minimum observed FWHM in our experiments. Since the 510nm Cu(I) line and 481nm Zn(I) line are not associated with a resonance state, the contribution from resonance broadening can be neglected. Stark broadening arises from the collision of the charged species. The Stark broadened emission line has a typical Lorentzian profile. The 510nm Cu(I) line and 481nm Zn(I) line emission line profile were fitted with a Lorentz function in order to estimate the full width at half maximum FWHM. The FWHM $\Delta\lambda_{1/2}$ of the Stark broadened profile is related to the electron number density n_e by the expression [26]:

$$\Delta\lambda_{1/2} = 2\omega\left(n_e/10^{16}\right) + 3.5\,A\left(n_e/10^{16}\right)^{1/4}\left[1 - \frac{3}{4}n_D^{-1/3}\right]\omega\left(n_e/10^{16}\right) \quad (5)$$

where ω is the electron impact width parameter, A is the ion broadening parameter. The parameters ω and A are weak functions of temperature and are taken from literature [27]. n_D is the number of particles in the debye sphere and is given by

$$n_D = 1.72 * 10^9 \frac{[T_e(eV)]^{3/2}}{[n_e(cm^{-3})]^{1/2}}\ cm^{-3} \quad (6)$$

The first term in Eq.(5) represents the broadening due to electron contribution, whereas the second term is attributed to the ion broadening. The electric field that causes Stark effect in LIPs results primarily from collisions with electrons, along with small contributions from collisions with ions. Neglecting the small contribution of the ion impact broadening; Eq.(5) is reduced to

$$\Delta\lambda_{1/2} = 2\omega\left(n_e/10^{16}\right) \quad (7)$$

The spectral line shape is also corrected for instrumental broadening. There is an uncertainty of about 10% in the value of electron number density thus determined due to the uncertainties in the width measurement, the instrumental width deconvolution, and the electron impact parameter. Fig.4b shows the evolution of plasma electron density for Cu(I) 510.5nm and Zn(I) 481.1nm species as a function of time after the fs-laser pulse. It is difficult to obtain the electron density estimates at earlier times i.e < 100ns delay using the Stark broadening technique as the spectra is dominated by strong continuum emission. The electron density estimates are much higher at the initial delays and decrease much rapidly at the initial stage followed by relatively little variation at larger delays. This is due to the fast thermalization and recombination processes. The latter is mainly via collisional three-body recombination[28], the rate of which R_c is given by:

$$R_c = Z^3 \ln\sqrt{Z^2 + 1}\, T_e^{-9/2} n_e n_i \quad (8)$$

where Z is the charge state, T_e is the electron temperature, and n_i is the ion density. As the fs-LIP plume expands, recombination of electrons and ions sets in and this results in reduction in electron density. It is worth mentioning the difference in electron densities estimated using Cu(I) and Zn(I) emission lines (cf.Fig.4b). The

higher electron density estimated using the Cu(I) line (vis-à-vis Zn(I) line) may be due to the much higher heat of vaporization and vaporization temperature of copper than that of zinc, which makes the copper in the plasma at a high temperature. A power curve fit to the data shows that the electron number density decreases exponentially.

3.2c Validity of LTE

The above equations (1-7) are valid only if the plasma is in thermodynamic equilibrium (LTE). For the plasma to be in a state of LTE, the excitation and de-excitation rates between atomic and ionic states should be dominated by inelastic collisions with electrons, rather than by radiative processes, i.e the rate of collision induced transitions from excited levels m to bound levels higher than m is much higher than the radiative decay rate(A_{jm}) to the level m.

$$e + A(m) \leftrightarrow e + A(n) \quad (9)$$

$$N_m \sum_{j>m} X_{mj} \gg \sum_{j>m} N_j A_{jm} \quad (10)$$

The collisional rates involving the populations N_m and N_j and the coefficients X_{mj} and X_{jm} are related to each other by the expression:

$$N_j X_{jm} = N_m X_{mj} \quad (11)$$

$$\frac{X_{jm}}{X_{mj}} = \frac{N_m}{N_j} = \frac{g_m}{g_j} e^{\left(\Delta E_{jm}/kT\right)} \quad (12)$$

where g_m and g_j are the statistical weights of levels j and m respectively and ΔE_{jm} is the difference between these two levels. Eq (10) is equivalent to:

$$N_j \sum_{j>m} X_{jm} \gg \sum_{j>m} N_j A_{jm} \quad (13)$$

In Eq.(10) the contribution involving levels higher than $n = m + 1$ can be ignored since the collisional cross-sections and population in the excited levels decreases with increasing values of quantum levels. Thus Eq.(10) is reduced to:

$$N_m X_{mn} \gg N_n A_{nm} \quad (14)$$

The LTE condition is tested by the McWhirter criterion according to which the number of downward transitions per unit time and per unit volume due to collisions is at least 10 times larger than the RHS term of Eq.(14) [29]

$$N_n X_{nm} > 10 N_n A_{nm} \quad (15)$$

Using the relation between A_{nm}, absorption oscillator strength and Eq.(12), the McWhirter criterion is expressed as:

$$n_e^l(cm^{-3}) \geq 1.6 * 10^{12} T_{ex}^{1/2} (\Delta E_{nm})^3 \quad (16)$$

where ΔE is the difference of energy between the excited and the lower state in eV (2.43eV for the 510.5nm Cu(I) transition), T_{ex} is the electron temperature in Kelvin and n_e^l is the lower limit of electron density. Using our measured value of temperature, 7296K at a detection delay of ~ 900ns, the estimated value of electron density n_e from the Stark broadened line profile is 1.54×10^{16}cm^{-3}, whereas the corresponding value from McWhirter criterion is 1.96×10^{15}cm^{-3}, thereby justifying the use of LTE.

It is also important to verify the second condition that the plasma should be optically thin for the lines that are used for its characterization. This is verified by measuring the intensity ratios of the non resonant Cu lines at 515.3nm, 521.8nm and 578.2nm, triplet of Zn emitting at 468.0nm, 472.2nm, and 481.0nm. The ratios of these lines are consistent with the ratio of the statistical weights of the upper energy levels.

3.3. Effect of fluence on plasma parameters

These set of experiments were carried out to understand the effect of the laser fluence on the plasma parameters. The fluence was calculated from measurements of beam average power, pulse repetition rate and

focal length of the lens imaging on the target. For a Gaussian laser-beam energy profile, the beam can be focused by a lens of focal length f to a waist radius $\omega_0^{'} = \frac{M^2 2\lambda f}{\pi D}$ on the substrate, where D is the diameter of the beam on the lens. The beam quality factor M^2 was estimated from aperture measurements over a long distance of beam propagation; in our case $M^2 = 1.08 \pm 0.2$. The peak fluence F_p on the beam axis can be estimated as $F_p = \frac{2E}{\pi\omega_0^{'2}}$, where E is the pulse energy.

The brass sample was ablated at different laser fluences ranging from 1.5 – 14 J/mm^2. Fig.5a shows the variation of the spectral emission intensity for Cu(I) line at 510.5nm as a function of applied fluence. The emission intensity of spectral lines is proportional to $Nexp(-E/kT)$ where N is density of atoms, E is the

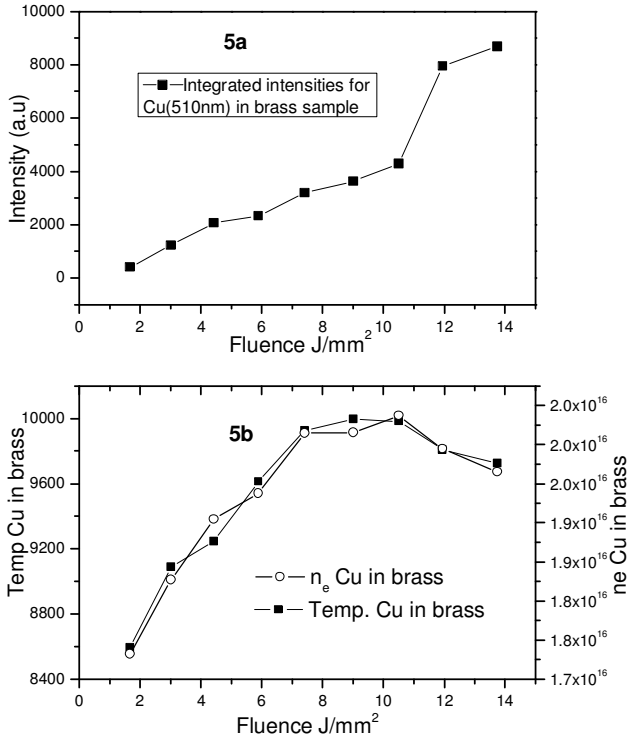

Fig.5a Variation of spectral emission intensity for Cu(I) (510.5nm) in brass sample as a function of laser fluence
Fig.5b Variation of plasma temperature and electron number density for Cu(I) (510.5nm) in brass sample as a function of laser fluence

energy of the upper level of the transition corresponding to the particular emission line and T is the plasma temperature. Therefore with increasing laser fluence, the number density of species emitting at an energetic atomic line (i.e the LIP intensity) increases unless the total mass of atoms substantially decreases. However, we see two different dependencies of spectral intensities on fluence corresponding to the two ablation regimes low fluence (1.5 – 9 J/mm^2) and high fluence (9– 14 J/mm^2). The different regimes of laser mater interaction are related to the three characteristic time scales τ_e the electron cooling time,τ_i, the lattice cooling time and τ_p, the duration of the laser pulse. The evolution of the absorbed energy involves thermalization within the electron gas (electron subsystem), energy transfer to the lattice and thermal diffusion in the lattice. In ultra short pulse laser ablation, the energy is assumed to be deposited as a delta function in time, the ultra-fast dynamics of such interactions is explained by the two temperature model (TTM) which involves solving two coupled differential equations for the electron and lattice temperatures [31]. In the low fluence regime the density of hot-electrons is

so low that the energy penetration depth (hence the ablation rate) is controlled by the optical absorption length. Nielsen *et al* [32] had observed a similar trend for ablation rates. By neglecting heat diffusion in both the lattice and the electron system, they proposed an analytical expression which gave a logarithmic dependence of the ablation rate with respect to laser fluence. In the high fluence regime, we find that temperatures were much higher compared to the low-fluence case (Fig.5b). At higher fluences heat propagation effects set in and the energy is distributed over hundreds of nanometers. The electron-lattice equilibrium is established after few tens of picoseconds [32]. The analytical expression proposed by Nielsen *et al* for the high-fluence regime assumes that most of the heat transport occurred in thermal equilibrium between electrons and lattice; the ablation rate exhibited a linear dependence on fluence. As the LIP emission intensity corresponds well with the mass removal rate during the laser ablation process [33], the two regimes shown in Fig.9 can be compared to analytical expressions derived from approximations to the two temperature model.

Further we see that at very high fluences (>11 J/mm^2) the ablation rate tends to saturation with increasing laser fluence. This is not due to plasma shielding and screening effects but due to the fact that as the crater depth increases with fluence, at a certain depth the characteristic time during which the melt attains the critical velocity for ejection becomes longer than the time it takes for the melt to cool down and resolidified according to the so called "piston model" [34,35]. Further, the variation of excitation temperature and electron number density as a function of laser fluence has been plotted in Fig.5b. As the laser fluence increases from 1.50–10.5 J/mm^2, n_e increases from 1.73*10^{16} to 2.04*10^{16} cm^{-3}, and T_e varies from 8592 to 9982 K. At the lower fluence levels (1.50 – 7 J/mm^2), the mass ablation rate increases rapidly with the increase in the laser power, thereby generating more free electrons, ions and excited species, hence increase in spectral line intensities and the spectral width. Hence the obvious increase in n_e and T_e. However, at higher fluence levels (> 8.0 J/mm^2), the increase in plasma temperatures and electron densities is very slow gradually tending to saturation; this can be explained on the basis of the piston model as described above.

We then extended these studies to investigate the behavior of plasma parameters in the simplest complicated matrix, brass (a two component system Cu and Zn) relative to matrix with only one major component (copper sample). To this end, we compared the behavior of copper emission lines in fs laser ablated brass and copper plasma. Identical ablation parameters were used in both the cases. The intensities and width of the Cu(I) emission lines is almost same in both cases. Figs.6a and 6b show the temporal evolution of plasma temp and electron density in both cases. They exhibit similar trends thus inferring that the optical penetration depth did not change with the change in concentration of the emitting element (Cu). This suggests that fs-laser pulses might mitigate the matrix effect in the ablation process.

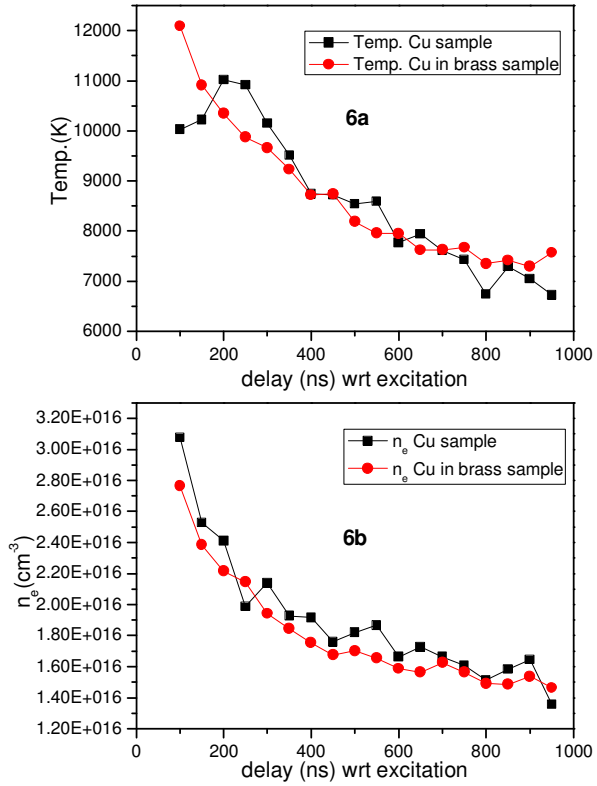

Fig.6a Temporal evolution of plasma temperature for Cu(I) species in copper and brass samples
Fig. 6b Temporal evolution of electron density using Cu(I) (510.5nm) transition in copper and brass samples

4. Conclusion

We have carried out a systematic investigation of the kinematic and radiative properties of fs-laser ablated brass plasma by applying optical emission spectroscopy (OES). The time and space integrated fs-LIP spectra was found to be dominated by emission from excited neutral species of Cu and Zn; the ionic species Cu(II) and Zn(II) had comparatively meagre intensities. The time-resolved emission data further revealed that ionic emission lines had shorter persistence compared to the atomic emission lines. The temporal evolution of prominently observed Zn(I) transition at 481.1nm and Cu(I) transition at 510nm showed a lifetime of 172ns and 303ns respectively. Assuming local thermodynamic equilibrium (LTE), the fs-LIP source was characterized for excitation temperature and electron number densities by using the Boltzmann plot method and the width of the Stark broadened line profiles respectively. Both these parameters have been studied as a function of time delay with respect to the excitation with a view to optimize them for quantitative analysis.

The influence of laser fluence on plasma parameters was also investigated. The results showed the presence of two different ablation regimes. The ablation at low fluences, is dominated by optical penetration depth whereas at high fluences electron thermal diffusion length plays a major role. The behavior of copper emission lines in fs laser ablated brass and copper plasma vis-à-vis the temporal evolution of plasma temp and electron density was almost the same in both cases. This suggests that ablation with fs-laser pulses might lead to reliable determination of elemental composition in solids.

Acknowledgement

We gratefully thank Dr D. K. Palit, Head, Radiation & Photochemistry Division and Dr B. N. Jagatap, Director, Chemistry Group, BARC, Mumbai for their keen interest and continued support.

REFERENCES

[1] A. W. Miziolek, V. Pallesch, I. Schechter, *Laser-Induced Breakdown Spectroscopy (LIBS): Fundamentals and Applications*, Cambridge University Press, (2006)

[2] D. A. Cremers, L. J. Radziemski, J. Wiley, *Handbook of Laser-Induced Breakdown Spectroscopy*, John Wiley & Sons, (2006)

[3] X. Hou, B. T. Jones, "Field Instrumentation in Atomic Spectroscopy", *Microchem. J.*, **66**, 115-145 (2000)

[4] R. E. Russo, T. W. Suen, A. A. Bol'shakov, J. Yoo, O. Sorkhabi, X. Mao, J. Gonzalez, D. Oropeza, V. Zorba, "Laser plasma spectrochemistry", *J. Anal. At. Spectrom.*, **26**, 1596-1603 (2011)

[5] B. Smith, "25 years of lasers and analytical chemistry: A reluctant pairing with a promising future", *Trends Anal. Chem.*, 26, 60-64 (2007)

[6] B. N. Chichkov, C. Momma, S. Nolte, F. Von Alvensleben, A. Tunnermann, "Femtosecond picosecond and nanosecond laser ablation of solids", *Appl. Phys. A: Mater. Sci. Process*, **63**, 109 (1996)

[7] Q. Yu, L. Li, E. Zhu, W. Hang, J. He, B. Huang, "Analysis of solids with different matrices by buffer-gas-assisted laser ionization orthogonal time-of-flight mass spectrometry", *J. Anal. At. Spectrom.*, *25*, 1155-1158 (2010)

[8] S. Link, C. Burda, B. Nikoobakht, M.A. El-Sayed, "Laser induced shape changes of colloidal gold nanorods using femtosecond and nanosecond laser pulses", *J. Phys.Chem. B*, **104**, 6152-(2000)

[9] E. Cromwell, P. Arrowsmith, "Fractionation effects in laser ablation inductively coupled plasma mass spectrometry", *Appl. Spectrosc.,* **49**, 1652-1660 (1995)

[10] H. L. Xu, G. M´ejean, W. Liu, Y. Kamali, J. F. Daigle, A. Azarm, P. T. Simard, P. Mathieu, G. Roy, J. R. Simard, S. l. Chin, "Remote detection of similar biological materials using femtosecond filament induced breakdown spectroscopy", *Appl. Phys. B*, **87**, 151-156 (2007)

[11] R. Le Harzic, N. Huot, E. Audouard, C. Jonin, P. Laporte, S. Valette, A. Fraczkiewicz, R. Fortunier, "Comparison of Heat affected Zone due to nanosecond and femtosecond laser pulses using Transmission Electronic Microscopy", *Appl. Phys. Lett.*, **80**, 3886-3888, (2002)

[12] S. Sreedhar, G. Manoj Kumar, M. Ashwin Kumar, P. Prem Kiran, P. Tewari Surya, S. Venugopal Rao, "Femtosecond and nanosecond laser induced breakdown spectroscopic studies of NTO, HMX, and RDX", *Spectrochim. Acta Part B,* **79-80**, 31-38 (2013)

[13] R. Hergenroder, O. Samek, V. Hommes, "Femtosecond laser-ablation elemental mass spectrometry", *Mass Spectrom. Rev.*, **25**, 551-572 (2006)

[14] R. E. Russo, X. L. Mao, C. Liu, J. Gonzalez, "Laser assisted plasma spectrochemistry: laser ablation", *J. Anal. At. Spectrom.* **19,** 1084-1089 (2004)

[15] M. Lenzner, F. Krausz, J. Kruger, W. Kautek, "Photoablation with sub-10 fs laser pulses", *Appl. Surf. Sci.,* **154,** 11-16 (2000)

[16] J. Gonzalez, C. Liu, X. Mao, R. E. Russo, "UV-femtosecond laser ablation-ICP-MS for analysis of alloy samples", *J. Anal. At. Spectrom.,* **19,** 1165-1168 (2004)

[17] J. Koch, D. Gunther, "Femtosecond laser ablation inductively coupled plasma mass spectrometry: achievements and remaining problems", *Anal. Bioanal. Chem.,* **387**, 149-153 (2007)

[18] B. Zhang, M. He, W. Hang, B. Huang, "Minimizing matrix effect by femtosecond laser ablation and ionization in elemental determination", *Anal. Chem.*, **85**, 4507- 4511 (2013)

[19] NIST Atomic Spectral Database, http://physics.nist.gov

[20] L. J. Radziemski, D. A. Cremers, *Laser induced plasmas and applications*, eds Marcel Dekker, USA (1989)

[21] Y. Ushirozawa, K. Wagatsuma, "Excitation Mechanisms of Copper Ionic and Atomic Lines Emitted from a Low-Pressure Argon Laser-Induced Plasma", *Spect. Lett.*, **38**, 539-555 (2005)

[22] J. A. M. van der Mullen, "On the atomic state distribution function in inductively coupled plasmas—I. Thermodynamic equilibrium considered on the elementary level", *Spectrochim. Acta Part B*, **44**, 1067-1080 (1989)

[23] H. R. Griem, *Plasma Spectroscopy*, McGraw-Hill Inc., New York (1964)

[24] T. Fujimoto, *Plasma Spectroscopy*, Clarendon Press, Oxford (2004)

[25] H. R. Griem, *Spectral Line Broadening by Plasmas*, Academic Press, USA (1974)

[26] G. Bekefi, *Principles of laser plasmas*, Wiley, Interscience (1976)

[27] N. Konjevic, M. S. Dimitrijevic, W. L. Wiese, "Experimental Stark Widths and Shifts for Spectral Lines of Neutral Atoms"**,** *J. Phys. Chem. Ref. Data*, **13(3),** 619-647 (1984)

[28] M. Capitelli, A. Casawola, G. Colonna, A. DeGiacomo, "Laser-induced plasma expansion: theoretical and experimental aspects", *Spectrochim. Acta B*, **59**, 271-289 (2004)

[29] R. W. P. McWhirter, *Plasma Diagnostic Techniques*, Academic press (1965)

[30] P. W. Milonni, J. H. Eberly, *Lasers*, John Wiley and sons, New York (1988)

[31] S. I. Anisimov, B. L. Kapeliovich, T. L. Perel'man, "Electron emission from metal surfaces exposed to ultrashort laser pulses", *Soviet Physics Jetp-Ussr*, **39(2)**, 375-377 (1974)

[32] J. Byskov-Nielsen, J-M. Savolainen, M. S. Christensen, P. Balling, *Appl. Phys. A,* **101**, 97-101 (2010)

[33] A. Fernandez, X. L. Mao, W. T. Chan, M. A. Shannon, R. E. Russo, "Correlation of spectral emission intensity in the inductively coupled plasma and laser induced plasma during laser ablation of solid samples", *Anal. Chem*., **67**, 2444-2450 (1995)

[34] A. Ruf, D. Breitling, P. Berger, F. Dausinger, H. Hügel, "Modeling and investigation of melt ejection dynamics for laser drilling with short pulses", *Proc. SPIE***,** 4830, 73-78 (2003)

[35] N.G. Semaltianos,·W. Perrie, P. French, M. Sharp, G. Dearden, S. Logothetidis,· K.G.Watkins, "Femtosecond laser ablation characteristics of nickel-based superalloy C263", *Appl. Phys. A*, **94**, 999–1009 (2009)